UNIVERSITY OF CALIFORNIA
RIVERSIDE

A Geochemical Study of the 1.4 Ga Roper Group, Northern Australia: A Window to Environmental Conditions and Life During the Mid-Proterozoic

A Thesis submitted in partial satisfaction
of the requirements for the degree of

Master of Science

in

Geological Sciences

by

Kevin D. Nguyen

December 2014

Thesis Committee:
Dr. Timothy W. Lyons, Chairperson
Dr. Gordon D. Love
Dr. Andrey Bekker

The Thesis of Kevin D. Nguyen is approved:

Committee Chairperson

University of California, Riverside

Acknowledgments

I would like to thank Dr. Alan Williams who introduced me to geology; I would have walked a different path had it not been for him.

Most importantly, I would like to give special thanks to Tim Lyons for all he has done. From our many trips together—the Salton Sea, Salvation Mountain, Glacier Park, Idyllwild, and the Grand Canyon—I owe him an unquantifiable amount of gratitude for taking a chance with me. Thank you to Gordon Love for graciously accepting me into his lab, and for giving me another powerful set of tools from which I can draw from. Thank you Dr. David Oglesby and Mary Droser for being there since the beginning of my graduate career.

I consider myself fortunate to be among such amazing company for the past two and a half years. To Dalton Hardisty, my graduate experience would not have been the same without you. Thanks for showing me how to channel my anger and frustration into productivity. To Jeremy Owens, thank you for being my mentor (if only briefly) and a friend—the office is not the same ever since you left. Thank you Steve Bates for being the best lab coordinator anyone can have—you are a modern day Macgyver. I also owe big thank you to all the lab help I received: Megan Rohrssen, Emily Haddad, Rosemarie Bisquera, Alexander Zumberge, Petra Schoon, Alexandra Ruiz, Carly Gott, Daisy Sim, Bridget Lee, Leanne Handcock, Andy Robinson, Natascha Riedinger, and Laura Wehrmann. Thank you Konstantin Choumiline for being the life of Lyons Group. Thank you Amy Kelly for giving me these samples on a silver platter and for all the guidance.

Thank you also to Michael Dahl for instilling in me a work ethic— that I can rest when I die and for those philosophical chats about life in general during carpool.

Another big thank you to John Herring, Louise DeHayes, Jennifer Reising, and Laurie Graham for keeping the department running like a well-oiled machine.

To my teachers: Mr. Dustin Tran, Mr. Nghiem Phu Phi, and Mr. Matthew Cain. Thank you for enriching my life academic, music, and chemistry.

Last but definitely not least, I would like to thank my parents for their constant love and support. To Melissa Ruiz, thank you for being my center of gravity—words cannot express how grateful I am that you stuck by my side and for that, I am the luckiest person in the world.

Dedication

For my parents and Melissa—I am very lucky.

ABSTRACT OF THE THESIS

A Geochemical Study of the 1.4 Ga Roper Group, Northern Australia: A Window to Environmental Conditions and Life During the Mid-Proterozoic

by

Kevin D. Nguyen

Master of Science, Graduate Program in Geological Sciences
University of California, Riverside, December 2014
Dr. Timothy W. Lyons, Chairperson

By about 2.0 billion years ago (Ga), there is evidence for a period best known for its extended, apparent geochemical stability expressed famously in the carbonate-carbon isotope data. Despite the first appearance and early innovation among eukaryotic organisms, this period is also known for a rarity of eukaryotic fossils and organic biomarker fingerprints, suggesting low diversity and relatively small populations compared to the interval that followed. Nevertheless, the search for diagnostic biomarkers has not been performed within an independent paleoenvironmental context that should reveal the facies that were most likely hospitable to these oxygen-requiring organisms. Shales and mudstones obtained from drill core of the ca. 1.45 Ga Roper Group from the McArthur Basin of northern Australia provide one of our best windows into the mid-Proterozoic redox landscape. The group is well dated and minimally metamorphosed, and previous geochemical data show a relatively strong connection to the open ocean compared to other mid-Proterozoic records. Consequently, conditions

captured in the Roper Group may better reflect the redox state of the ocean margin and may reveal eukaryote-favoring setting. Despite this potential, a comprehensive, multi-proxy study of the Roper Group had not been undertaken. Here we present one of the first integrated investigations of Precambrian biomarkers performed within a strict inorganic proxy context. Results show a textured paleoredox structure for the Velkerri Formation, vacillating between oxic and anoxic, even euxinic conditions in the water column. Despite this variability, including the likely presence of oxic bottom waters, we see no evidence for the sterane compounds that would point convincingly to the presence of eukaryotes in this marine basin roughly 1.45 Ga. Also missing are the aryl isoprenoids that would delineate shallow photic zone euxinia and thus the likelihood of appreciable anoxygenic primary production, even though the iron and trace metal data are consistent with the presence of euxinia deeper in the water column. The absence of eukaryotic signals—despite our search across oxic and anoxic facies that should favor their habitability and the preservation of their records, respectively—suggests that other controls such as long-term nutrient and oxygen deficiencies may have throttled the distributions and diversity of early complex life.

Table of Contents

List of Figures

List of Tables

INTRODUCTION

The mid-Proterozoic is well known for its long-lived geochemical stasis, showing only subtle variation in carbonate $\delta^{13}C$ spanning this interval (Brasier and Lindsay, 1998). By this time, eukaryotes had emerged and diversified (Knoll et al., 2006), but their evolutionary development was apparently stifled so that diversity patterns and abundances were persistently low compared to the later Neoproterozoic (Knoll et al., 2006). Past work has suggested that low oxygen contents and related limited availability of critical nutrients in the ocean may have contributed to the apparent biogeochemical and paleobiological stasis (Lyons et al., 2014; Reinhard et al., 2013). Despite important innovations during this interval, this apparent monotony relative to the events that followed has led to the common referral of the period 2.0 and 0.8 Ga as the "dullest time in Earth's history" (Buick et al., 1995).

Our current understanding of the redox chemistry of the mid-Proterozoic ocean is that the surface waters were most likely oxygenated, while the deeper low-oxygen waters were marked by sulfidic (euxinic) zones at intermediate depths, particularly along the highly productive ocean margins. Iron-rich anoxic (ferruginous) conditions dominated at greater depth (Lyons et al., 2009). The redox structure of the ocean at that time controlled the patterns and rates of evolution by modulating the spatiotemporal distribution of essential macro- and micro-nutrients, as well as overall availability of oxygen (Reinhard et al., 2013; Scott et al., 2008). It has been suggested that biological feedbacks, including sulfide-based anoxygenic photosynthesis (Johnston et al., 2009), would tend to maintain a world in which oxygen levels were low and sulfide levels were high to the point of

limiting the development and proliferation of early complex life. However, various feedbacks make the persistence of widespread anoxia, particularly euxinia, equally challenging. Specifically, nutrient limitations coupled to widespread anoxia and euxinia (e.g., loss of fixed nitrogen through denitrification and limited availability of the trace metal micronutrients such as molybdenum that are critical in offsetting nitrogen fixation) can result in reduced availability of organic matter required to sustain anoxia via aerobic respiration and to support sulfide production via microbial sulfate reduction (Lyons and Reinhard, 2009; Scott et al., 2008). The apparent balance among these feedbacks that kept the mid-Proterozoic ocean "dull" remains a topic ripe for further study.

It is widely accepted that the chemistry of the early ocean and its life co-evolved. However, the true geochemical nature of Earth's "boring billion" remains poorly constrained. There are many lines of evidence that document an increase in Earth's surface oxidation state approximately 2.4 to 2.3 Ga (Bekker et al., 2004; Lyons et al., 2014), and another biospheric oxygenation estimated between 800 to 550 Ma (Och and Shields-Zhou, 2012; Sahoo et al., 2012) that was coincident with the arrival of animals. Conditions in the intervening mid-Proterozoic are less studied and correspondingly less known, with the likelihood of intermediate redox states in the ocean and atmosphere. Many of the most-cited data have come from the McArthur Basin of northern Australia. Specifically, shales and mudstones of the Roper Group in this region have emerged as one of our best archives of mid-Proterozoic ocean redox because the group is well dated, minimally metamorphosed, and lie in the middle of this key interval (Jackson et al., 1988). Most importantly, sedimentological and geochemical data suggest a relatively

strong connection to the open ocean (Jackson et al., 1988; Jackson et al., 1986; Jackson and Raiswell, 1991). As a result, conditions in the Roper Group may reflect the redox state of the global ocean and specifically the conditions that favored, or challenged, the development and expansion of complex life during this interval. Given this potential, we herein report on the first high-resolution, fully integrated geochemical study of the Roper Group—with the goal of performing organic biomarker work within a tight inorganic geochemical context that defines a gradient in habitability and thus potential eukaryotic inhabitation. Our results suggest that controls other than local redox modulated the distribution of eukaryotic organisms in the mid-Proterozoic ocean.

SAMPLING LOCATION AND LITHOLOGY

Much of the attention drawn to the McArthur Basin was through the discovery of "live oil" originally reported by (Jackson et al., 1986). Their findings garnered significant interest in the area, and subsequent investigations have been designed to define its depositional environment. Concisely, the Roper Group within the McArthur Basin is located at the tip of northern Terrirtory of Australia, near the Gulf of Carpentaria, and occurs over an area of at least 145,000 km^2 with a maximum thickness of approximately 5000 m (Abbott and Sweet, 2000). The samples in this study are from the Velkerri Formation sampled in the Altree-2 drill core; the Velkerri has a known extent of at least 80,000 km^2 (Jackson and Raiswell, 1991). (Jackson et al., 1999) reported U-Pb age of 1.492 ± 4 Ma from the lowermost member of the Roper Group, the Mainoru Formation. The Altree-2 drill core was sampled over a depth interval of 440 – 1250 m, covering the full thickness of the Velkerri Formation. The formation is divided into three informal

subunits—the upper, middle, and lower Velkerri. Starting with the upper Velkerri, samples spanning 441 – 666 m are comprised of shale with minor laminated and interbedded mudstone. The middle Velkerri is covered by samples spanning from 705 – 933 m and consists of shale grading to mudstone. Lastly, the lower Velkerri—with samples spanning from 1000 to 1130 m—is comprised of mudstone grading locally to shale, with the remaining 1130 – 1242 m comprised of mudstone interbedded with very fine sandstone.

METHODS

Sampling specifically targeted shales and mudstones in drill core to explore the degree of oxygenation within the local water column and to provide added perspective on oxygen in the global ocean. Total carbon (TC), total inorganic carbon (TIC), and total sulfur (TS) were measured by infrared absorption of CO_2 using an Eltra CS-500 equipped with a furnace and acidification module. TC and TS were determined via combustion at 1400° C, while TIC was liberated via reaction with 4N HCl. Total organic carbon (TOC) was calculated by difference.

Sequential extraction of reactive Fe phases was carried out using the previously described method (Poulton and Canfield, 2005) and analyzed on a Agilent 7500ce quadrupole inductively coupled plasma mass spectrometer (ICP-MS). Reproducibility of Fe speciation measurements, based on replicate analyses within and between sample batches, was better than 93%.

Pyrite iron (Fe_{Py}) was quantified using chromous chloride distillation followed by titration with iodine as outlined in (Canfield et al., 1986). A pyrite standard was utilized

in every sample batch, averaging 76% recovery with a standard deviation of 7.8 %. Iron relationships were also assessed using the conventional degree of pyritization technique (DOP) (Raiswell et al., 1988), whereby residual (unpyritized) 'reactive' Fe is extracted using a boiling, 12N HCl step. This DOP technique will, if anything, overestimate the truly reactive phases. As such, false positives for euxinia are unlikely, and high DOP values are taken as a particularly robust indication of that condition in the ancient water column (see review in (Lyons and Severmann, 2006). Once extracted, the amount of iron was quantified spectrophotometrically using the standard ferrozine method. Replicate analysis yielded a standard deviation of 0.25 wt. %.

Pyrite sulfur in the samples was also extracted using the Cr reduction method for sulfur isotope analysis via a silver nitrate trap, rather than the zinc acetate solution used for the pyrite-S quantification by iodometric titration. The resulting silver sulfide was homogenized with excess V_2O_5 and combusted online for analyses of $^{34}S/^{32}S$ ratios using a Thermo Delta V mass spectrometer, which are reported using the delta notation as per mil (‰) deviations from the Vienna Canyon Diablo Troilite (VCDT) standard. Reproducibility was better than 0.14 ‰ based on single-run and long-term standard monitoring (additional analytical details for the DOP and $\delta^{34}S$ determinations are provided in the supplementary materials).

A multi-acid digestion technique was employed for trace-metal analysis. Samples were ashed at 900° C for 24 hours, and mass lost through ignition was recorded prior to undergoing acid digestion (HF, HNO_3, and HCl). Analyses were performed on same ICP-

MS with the Devonian Ohio Shale (SDO-1) as a reference, with reproducibility in individual runs of better than 95% for the presented elements.

For organic biomarker analysis, select samples were trimmed with a rock saw to expose a solid core and the resulting chips were solvent-rinsed prior to powdering. Lipid biomarkers were extracted in 9:1 vol/vol dichloromethane/methanol using a Microwave Accelerated Reaction System (CEM Corp.) and whole bitumens were separated into saturates, aromatics, and polar (N,S,O compounds) fractions by silica column chromatography. Gas Chromatography-Mass Spectrometry (GC-MS) was performed in full scan mode over a mass range of 50 to 600 Da on an Agilent 5975C inert Mass Selective Detector (MSD) mass spectrometer interfaced to an Agilent 7890A GC, equipped with a DB-1MS capillary column (60 m x 0.32 mm, 0.25µm film) and run in splitless injection mode with He as carrier gas. The temperature program for GC-MS full scan was 60ºC (2 min), ramped to 150ºC at 20ºC/min, then to 325ºC at 2ºC/min, and held at 325ºC for 20 min.

Metastable Reaction Monitoring Gas Chromatography-Mass Spectrometry (MRM GC-MS) was conducted with a Waters AutoSpec Premier mass spectrometer equipped with an Agilent 7890A gas chromatograph and DB-1MS coated capillary column (60m x 0.25 mm, 0.25µm film) using splitless injection and He for carrier gas to probe polycyclic alkane biomarker distributions in detail. The GC temperature program used for compound separation consisted of an initial hold at 60ºC for 2 min, heating to 150ºC at 10ºC/min followed by heating to 320ºC at 3ºC/min, and a final hold at 320ºC for 22 min. Biomarker compounds were identified based on retention time and published mass

spectra and quantified in MRM GC-MS by comparison with a deuterated C_{29} sterane internal standard (d_4-ααα-24-ethylcholestane (20R), Chiron Laboratories, AS), assuming equal response factors between sample compounds and the internal standard. Individual yields of hopane and sterane diastereoisomers found in laboratory procedural blanks were typically <0.2 ng of individual compounds.

RESULTS AND DISCUSSION

Figure 1.

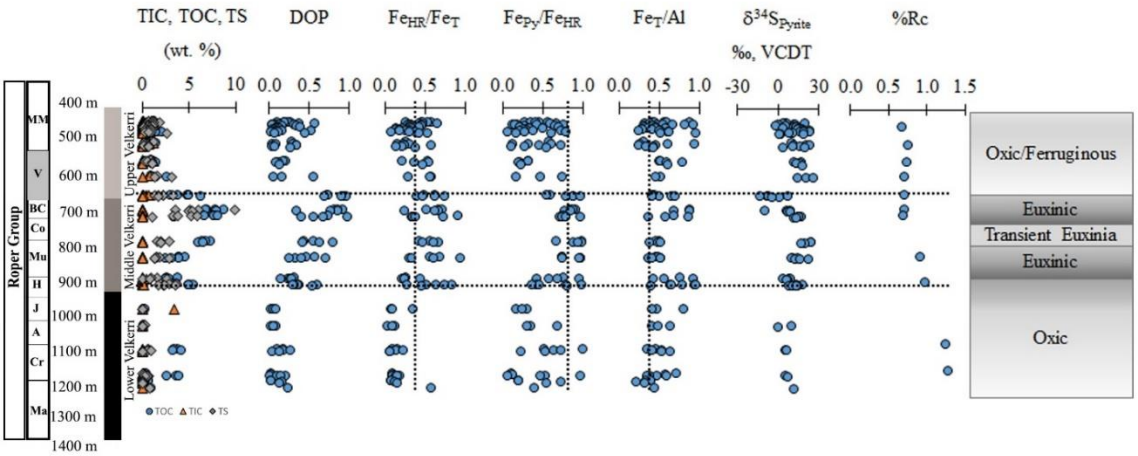

Stratigraphic column (emphasizing shales and mudstones) for drill core Altree-2 from the Velkerri Formation, Roper Group with stratigraphic variations of: TOC/TIC/TS; DOP; Fe_{HR}/Fe_T; Fe_{Py}/Fe_{HR}; Fe_T/Al; $\delta^{34}S_{Pyrite}$; %Rc; and a representation of the Velkerri Formation redox structure. Fe_{HR}/Fe_T ratios greater than 0.4 reflect anoxic deposition. Fe_{Py}/Fe_{HR} ratios above 0.8 reflect euxinic deposition (Poulton and Canfield, 2011). Fe_T/Al ratios below 0.4 to 0.5 reflect an oxic setting, while a ratio of 0.6 to 1.0 indicates anoxia/euxinia. Dashed line represents average oxic marine values for the Fe speciation data. TOC—total organic carbon; TIC—total inorganic carbon; TS—total sulfur; DOP – Degree of Pyritization; Fe_{HR}—highly reactive iron; Fe_T—total iron; Fe_{Py}—pyrite iron; %Rc—vitrinite reflectance equivalent.

Total Organic Carbon, Inorganic Carbon, and Total Sulfur

TOC content is abundant in most samples (Fig. 1), with values ranging from zero to as high as 8.8 wt. %. The lower Velkerri is marked by two episodes where TOC content hovers around 3.5 wt. % on average for a few meters relative to a baseline with near-zero values. The middle Velkerri shows higher TOC contents ranging from roughly 5.5 wt. % at 932 m to a maximum of 8.8 wt. % at 707 m, with a general up-core increase, before oscillating between very low values and 6.2 wt. % in the upper Velkerri. High organic content observed in the Velkerri Formation is interpreted to reflect high but varying organic carbon burial against a backdrop of relatively low clastic dilution (Warren et al., 1998). TIC content for the majority of the samples were unvaryingly low throughout the sequence, ranging from zero to 1.2 wt. %, with the latter equating to about 10% calcium carbonate. TS behaved similarly to TOC, ranging from values below detection to a maximum of 9.9 wt. % at 707 m in the middle Velkerri before tapering off to low concentrations ranging from values below detection to 1 wt. % in the upper Velkerri.

The Iron Paleoredox Proxies and $\delta^{34}S$

Highly reactive iron (Fe_{HR}) is comprised of pyrite iron (Fe_{Py}) and other iron-bearing phases that display a broad scale of reactivity towards sulfide in the water column and/or during early diagenesis—i.e., ferric (oxyhydr)oxides (Fe_{Ox}), magnetite (Fe_{Mag}), and iron associated with carbonate (Fe_{Carb}) (Poulton and Canfield, 2005). Modern marine sediments deposited beneath oxic waters exhibit Fe_{HR}/Fe_T ratios that average about 0.2 and seldom exceed 0.38, which is the upper limit for oxic deposition (reviewed in

Poulton and Canfield, 2011). Values above this threshold imply anoxic deposition (Raiswell and Canfield, 1998). The ratio for total iron to aluminum, Fe_T/Al, can also be used as an indicator for water column anoxia if Fe enrichments are significantly above the average for continental crust (Lyons and Severmann, 2006; Taylor and McLennan, 1985). If anoxia is indicated by high Fe_{HR}/Fe_T and Fe_T/Al ratios, the Fe_{Py}/Fe_{HR} ratio can further distinguish between anoxia and euxinia because under euxinic conditions, appreciable Fe^{2+} and solid highly reactive Fe phases cannot co-exist simultaneously with free H_2S in the water column—with the result of near-complete conversion of Fe_{HR} to pyrite and thus high Fe_{Py}/Fe_{HR} ratios.

Values for Fe_{HR}/Fe_T and Fe_T/Al in the lower Velkerri suggest oxic deposition (Fig. 1, tables in supplementary material), with ratios falling below 0.2 and slightly elevated above 0.4, respectively. Oxic deposition can be difficult to delineate using the iron proxies because rapid sedimentation can dilute the reactive Fe pool (as well as redox-sensitive trace metals)—specifically the enrichments that are diagnostic of anoxic conditions—via extreme detrital inputs (Lyons and Severmann, 2006). However, Fe_{HR}/Fe_T values in the middle and upper units are often elevated, and the persistence of shales/mudstones throughout all three subunit makes it difficult to argue for significant temporal changes in rates or patterns of sedimentation tied, for example, to varying water depth. Moreover, previous work has shown that comprehensive dilution of the Fe_{HR} enrichments that are diagnostic of anoxia seems to require extremely high rates of sedimentation (Lyons and Severmann, 2006). Although false positives for oxic deposition are possible, we should be able to recognize these extremes using standard

sedimentological and stratigraphic criteria. Finally, the presence of some high values for Fe_{Py}/Fe_{HR} in the lower interval, despite low Fe_{HR}/Fe_T, suggests sulfidic buildup in pore fluids beneath oxic bottom waters, as is observed in marine sediments today (Canfield et al., 1992). The higher observed organic contents of these thin intervals, relative to those immediately above and below, would have favored intense diagenetic pyrite formation.

A water column transition to euxinia in middle Velkerri is suggested by simultaneously elevated Fe_{HR}/Fe_T, Fe_T/Al, and Fe_{Py}/Fe_{HR}. These values taper off gradually at around 850 m and become pronounce again at 725 m, suggesting a transient euxinic phase followed by persistent euxinia. Euxinia is also convincingly indicated for this middle interval by high DOP values that approach 1.0 near the top (Fig. 1). The same upper portion of the middle interval is also marked by an obvious decrease in $\delta^{34}S$ values. Such isotopically light values can be interpreted to reflect a predominance of water column (euxinic) pyrite formation under more open-system conditions (Lyons, 1997). The remaining values show the typical ^{34}S enrichments seen commonly in the mid-Proterozoic, which are often attributed to generally low sulfate availability in the ocean at this time (Canfield et al., 2010; Kah et al., 2004; Shen et al., 2003). The heaviest value, +25.8 ‰, occurs in the upper Velkerri and closely matches a past estimate for the isotopic composition of the Roper seawater sulfate (Muir et al., 1985). Towards the upper Velkerri, values for Fe_T/Al remain elevated, while those of Fe_{HR}/Fe_T oscillates—suggesting ferruginous and oxic conditions. Ferruginous rather than euxinic conditions are confirmed by Fe_{Py}/Fe_{HR} ratios that are only intermediate in magnitude. Overall, the iron proxies reveal a textured paleoredox structure for Velkerri Formation—from oxic

grading toward euxinic in the lower Velkerri, then transiently euxinic to persistently euxinic in the middle Velkerri, and finally oscillating between ferruginous and oxic conditions in the upper Velkerri.

Figure 2.

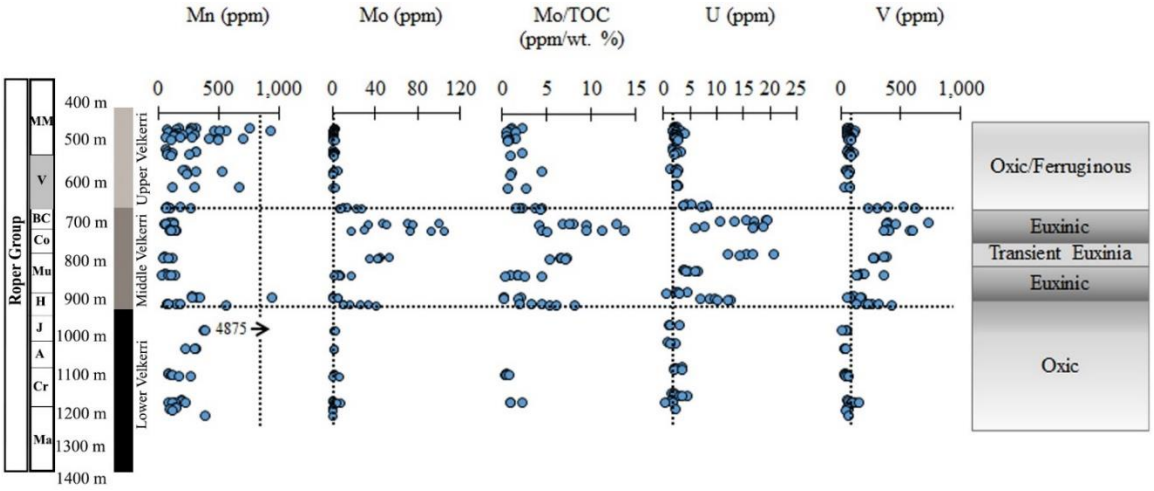

Stratigraphic column (emphasizing shales and mudstones) for drill core Altree-2 from the Velkerri Formation, Roper Group with stratigraphic variations of: Mn; Mo; Mo/TOC; U; V; and a representation of Velkerri Formation redox structure. Mo/TOC panel has been culled (TOC with values less than 1 wt. % were not included) to accurately reflect the co-variation. Dashed line in trace-metal panels represents average values of the continental crust. Mn—Manganese, Mo—Molybdenum, U—Uranium, V—Vanadium, TOC—total organic carbon.

Trace-Metal Proxies

Molybdenum (Mo), uranium (U), and vanadium (V) concentrations generally track TOC throughout the sequence (Fig. 2, tables in supplementary material) and are at crustal levels in the lower Velkerri and reach a maxima of 105 ppm for Mo and 21 ppm for U in the middle Velkerri. Similar values for Mo and U were previously observed from the same units by (Kendall et al., 2009) and (Partin et al., 2013), respectively. Mo, U, and V concentrations return to crustal levels in the upper Velkerri. Strong enrichment in Mo

convincingly argues for euxinic deposition because Mo burial is favored under reducing conditions marked by appreciable H_2S in the water column, with the lower enrichments being characteristic of sulfide that is confined to the pore waters (Scott and Lyons, 2012). Mo enrichment can also track the availability of organic carbon in euxinic systems (Algeo and Lyons, 2006), but we observe the same stratigraphic trend for Mo/TOC (Fig. 2)—suggesting that we are not missing a euxinic interval because of low TOC. Uranium and V on the other hand require a less reducing conditions and can be enriched in sediments marked by anoxic but not necessarily euxinic conditions (Tribovillard et al., 2006) (see supplementary material for a related discussion of V geochemistry and (Partin et al., 2013) for more background on U). Pronounced enrichments for all three metals, combined with the Fe proxy data, point convincingly to dominantly euxinic conditions in the middle Velkerri. The high-end concentrations for Mo and U in this interval are among the largest known for the mid-Proterozoic. Magnitudes of local Mo and U enrichment in euxinic sediments are controlled by the spatial extent of euxinia and anoxia in the global ocean (e.g., (Partin et al., 2013; Reinhard et al., 2013; Scott et al., 2008). As such, these relatively high Mo and U values may mark an transient oxidation event in the ocean-atmosphere system during the mid-Proterozoic (see (Reinhard et al., 2013).

Concentrations for Mo, U, and V above and below the middle interval are at near-crustal levels. Despite evidence for intermittently ferruginous waters in the upper part, Fe_{HR}/Fe_T ratios are generally low in both intervals. Collectively, the trace-metal and Fe speciation results imply common, at least moderate levels of marine oxygenation, locally and perhaps globally, throughout the Velkerri time of the mid-Proterozoic. Consequently,

these samples, for both local and global reasons, are particularly appropriate for our organic geochemical search for eukaryotes.

Consistent with our integrated, conceptual paleoredox model for the Velkerri Formation, manganese (Mn) concentration behaves antithetically to Mo, U, and V, exhibiting low values in the euxinic intervals and high values when the prevailing redox was dominantly oxic (lower Velkerri) or vacillating between ferruginous and oxic conditions (upper Velkerri). These Mn enrichments suggest greater Mn-oxide burial, implying appreciable oxygen in the water column (Calvert and Pedersen, 1993; Froelich et al., 1979). Furthermore, Mn appears to be tracking TIC, which we assume to reflect authigenic Mn-rich carbonate. In this case, the prerequisite for Mn-carbonate precipitation is oxic bottom waters where Mn oxides are trapped in the sediments and redox cycled repeatedly, resulting in dissolved Mn buildup in the subsurface anoxic portions of the pore water profile and subsequent carbon precipitation (Calvert and Pedersen, 1996; Calvert and Pedersen, 1993).

Organic Biomarkers

Operating within our inorganic geochemical framework can yield nuanced information that can resolve longstanding questions about the extent of mid-Proterozoic eukaryotic development, the environmental background, and the nutrient conditions of their early evolution. In this context, we look for possible biomarkers by targeting depths that had relatively high TOC (greater than 1 wt. %); high and low Mo concentrations; and facies overall that reflect varying depositional redox, including independent suggestions of at least intermittently hospitable oxic conditions in the bottom waters. Consequently,

selected samples cover most of the Velkerri Formation, ranging from 452 – 1205 m, (tables in supplementary material).

Although lipid biomarkers can contribute a better understanding of the mid-Proterozoic ocean chemistry and biology, there is also a drawback—because of the nature of mature Precambrian rocks; certain signals may sometime be indistinguishable from noise. As a result, contamination is the primary concern—from migration of hydrocarbons across a billion or more years of burial history, or from oil used to drill the cores. Fortunately, this can be abated through meticulous methodology designed to identify obvious contamination. E.g., methylphenanthrene index (MPI-1)—a maturity parameter, can check for systematic changes in the sample to ensure that the bitumen records have not been compromised by high thermal overprints (Radke and Welte, 1981). Recall that column chromatography separates the total lipid extract (TLE) into three fractions: saturates, aromatics, and polar. Only the saturate and aromatic fractions were analyzed for this study to generate various parameters such as hopane, sterane ratios; 2- and 3-methylhopane indices; and absolute yields of individual biomarkers (Table 1).

Detection of short chain *n*-alkane and hopane signals found in saturate fractions suggests a bacterially dominated ecology that drove primary productivity. Importantly, the robust presence of these compounds is inconsistent with loss of original steranes in our samples via thermal overprints. In addition, the aromatic fractions analysis performed by Geomark Research reported a lack of β-carotane and no aromatic carotenoid, below detection limit of 1-ppm carotenoid to micrograms/g aromatic fraction.

MPI-1 (Table 1) showed apparent linear correlations with depth—values began increasing from 0.49 at 725 m (middle Velkerri) to as high as 1.48 at 1205 m (lower Velkerri). This result is consistent with previous analyses of the same core (Summons et al., 1994). In addition, % Rc (vitrinite reflectance calculated from MPI-1) display the same linear trend (Fig. 1). Cross-checking with C_{27} hopanes 18α(H)-22,29,30-trisnorhopane II (Ts) and 17α(H)-22,29,30-trisnorhopane (Tm)—where Ts is the stable thermodynamic configuration and degrades into Tm with increasing temperature—a ratio where Ts/(Ts + Tm) approaches 1 represents an increase in maturity (Seifert and Michael Moldowan, 1978). In the Velkerri, Ts/(Ts + Tm) ratio is observed at 0.59 at 452 m (upper Velkerri), and increases to as high as 0.76 at 852 m (middle Velkerri). Moreover, moretanes (βα–isomers) are thermodynamically less table than the αβ-hopanes, thus their abundances should decrease relatively to thermal maturity. The low ratios of C_{30} βα–isomers/αβ–isomers observed in the Velkerri verifies that these rocks are not immature.

Another parameter that utilizes 2-methylhopanes, can be produced as major lipids by cyanobacteria and some soil proteobacteria (Summons et al., 1999). It has been shown that 2-methylhopane can be produced anoxygenically by a bacteria strain—*Rhodopseudomonas palustris* (Rashby et al., 2007). 2-MeH indices were as low as 1.7 % at 508 m (upper Velkerri) and as high as 8.2 % at 725 m (middle Velkerri).

3-methylhopanes on the other hand, are produced by Type I methanotrophic proteobacteria and acetic acid bacteria (Farrimond et al., 2004). Thus, a high ratio of C_{31} 3-methyhopane index can act as a proxy for past aerobic methanotrophic activity. 3-MeH

indices were as low as 1.6 at 561 m (upper Velkerri) and as high as 9.5 % at 706 m (middle Velkerri). Interestingly, high 3-MeH indices (average 5.7 %) were observed in the Barney Creek Formation (Brocks et al., 2005), suggesting high levels of aerobic methane oxidation. However, it is important to note that not all methanotrophs actually produce 3-MeH, such as Type II methanotrophic bacteria. Thus, high 3-MeH may not truly reflect the levels of methane activity, perhaps even underestimating it. (Brocks et al., 2005) also reported evidence for green and purple sulfur bacteria, reflecting photic zone euxinia, in rocks of the 1.64 Ga Barney Creek Formation also from the McArthur Basin. In contrast, the Velkerri Formation shows a lack of aryl isoprenoids and C_{40} parent carotenoid markers for anoxygenic phototrophic bacteria, consistent with a lack of photic zone euxinia.

Across this full gradient in ocean chemistry, we found very low to no evidence near detection limit for steranes, as observed in the C_{27}Sterane and C_{21+22}Sterane ratios—even in the relatively more oxic facies, suggesting that eukaryotes were not abundant during this mid-Proterozoic period in Earth history compared to the later Proterozoic. Previous models have asserted that low nutrient availability and associated deficiencies in oxygen may have throttled early diversity and abundances of eukaryotes (Anbar and Knoll, 2002; Javaux et al., 2001; Lyons et al., 2014; Reinhard et al., 2013). With our new results, we can comfortably assert that the absence of diagnostic biomarkers for eukaryotic organisms is not a product of locally inhospitable conditions due to low oxygen content. The suggestion, then, is that the environment of the Velkerri Formation may have been anomalously favorable—marked by at least episodically hospitable waters

during an interval in Earth history more generally characterized by delayed eukaryotic proliferation in more prominently inhospitable oceans, despite important early steps in innovation. In other words, the Velkerri Formation provides an ideal environmental window to sample the global, evolutionary state of complex life—free of local redox bias—yet a fundamental conclusion is that eukaryotes did not make significant contributions to the sedimentary organic matter deposited in the McArthur Basin suggesting that eukaryotes were not abundant marine primary producers during this interval of the mid-Proterozoic.

Table 1.

Depth (m)	TOC (wt. %)	MPI	%Rc	Ts/Tm	Ts/(Ts+Tm)
452.14-.22	1.5	0.45	0.67	1.43	0.59
508.35-.44	1.4	0.59	0.75	1.60	0.62
561.58-.64	1.2	0.57	0.74	1.73	0.63
607.91-.98	2.6	0.53	0.72	1.10	0.52
663.83-.91	5.0	0.51	0.71	1.66	0.62
706.87-.96	7.8	0.51	0.71	1.95	0.66
725.76-.88	7.6	0.49	0.69	2.92	0.74
852.68-.76	3.3	0.85	0.91	3.11	0.76
932.88-.92	5.5	0.96	0.98	1.70	0.63
1125.55-.57	3.4	1.41	1.25	-	-
1205.18-.20	3.9	1.48	1.29	-	-

Depth (m)	C29αβ/C30αβ	C30βα/C30αβ	C31αβ S/(S + R)
452.14-.22	0.89	0.07	0.55
508.35-.44	0.71	0.06	0.57
561.58-.64	0.69	0.06	0.59
607.91-.98	0.72	0.05	0.52
663.83-.91	0.74	0.06	0.58
706.87-.96	0.89	0.06	0.57
725.76-.88	0.53	0.05	0.55
852.68-.76	0.81	0.09	0.64
932.88-.92	0.51	0.08	0.55
1125.55-.57	-	-	-
1205.18-.20	-	-	-

Depth (m)	2αMeH Index (%)	3βMeH Index (%)
452.14-.22	5.9	2.4
508.35-.44	1.7	5.6
561.58-.64	2.4	1.6
607.91-.98	5.9	2.7
663.83-.91	7.1	5.9
706.87-.96	5.3	9.5
725.76-.88	8.2	3.0
852.68-.76	5.3	2.9
932.88-.92	2.8	8.5
1125.55-.57	-	-
1205.18-.20	-	-

Depth (m)	2αMeH Yield (ng/g TOC)	3βMeH Yields (ng/g TOC)
452.14-.22	0.05	0.02
508.35-.44	0.01	0.05
561.58-.64	0.01	0.01
607.91-.98	0.01	0.00
663.83-.91	0.17	0.14
706.87-.96	0.46	1.24
725.76-.88	0.03	0.01
852.68-.76	0.01	0.01
932.88-.92	0.01	0.03
1125.55-.57	-	-
1205.18-.20	-	-

Depth (m)	C27St//C30αβ	C21 + C22St/C30αβ
452.14-.22	0.00	0.00
508.35-.44	0.00	0.00
561.58-.64	0.00	0.00
607.91-.98	0.00	0.00
663.83-.91	0.00	0.00
706.87-.96	0.00	0.00
725.76-.88	0.00	0.00
852.68-.76	0.00	0.00
932.88-.92	0.00	0.00
1125.55-.57	-	-
1205.18-.20	-	-

Selected lipid biomarker ratios for Precambrian rock extracts. MPI, %Rc, Ts/Tm, Ts/(Ts+Tm), $C_{29}H/C_{30}H$, $C_{30}M/C_{30}H$, $C_{31}H$ 22S/($C_{31}H$ 22S + $C_{31}H$ 22R), C_{31} 2aMeH/(C_{31} 2aMeH + $C_{30}H$), C_{31} 3bMeH/(C_{31} 3bMeH + C30H), $C_{27}St$//C30H, $C_{21}St$ + $C_{22}St/C_{30}H$. MPI—methylphenanthrene index, %Rc—vitrinite reflectance equivalence, Hopane—H, Sterane—St, MeH—Methylhopane.

CONCLUSIONS

Iron and trace-metal data from the Velkerri Formation reveal that there was more apparent temporal variability in the marine redox conditions during the mid-Proterozoic than was previously recognized through analysis of the same interval (Kendall et al.,

2009; Shen et al., 2002; Shen et al., 2003). Overall, the system appears to have evolved from one that was dominantly oxic during deposition of the lower Velkerri Formation to euxinic in the middle Velkerri. More specifically, the middle unit is marked by evidence for a transient period of euxinia before evidence for water column sulfide that persisted to the upper Velkerri, as supported by the combined Fe and Mo data. The upper Velkerri Formation shows an intriguing combination of low trace metal abundances but numerous Fe speciation data suggesting frequent ferruginous but not euxinic deposition—with other Fe speciation data that are more reasonably attributed to oxic conditions. The lack of U and V enrichment places possible constraints on the limited duration of the anoxic conditions—and the relative rates of U and V versus Fe enrichment—and the possibility of V and U remobilization under conditions of rapid redox variability (and subsequent oxic overprints specifically). The Fe signatures of ferruginous conditions, by contrast, could be retained even if reduced Fe phases were oxidized. (In fact, episodes of euxinia could be masked this way [with spurious signatures for ferruginous waters] through penecontemporaneous pyrite oxidation.) The bottom line for the upper interval, however, is one of oscillatory redox between oxic and anoxic deposition.

More recently, an emerging view of the mid-Proterozoic ocean redox was presented in (Planavsky et al., 2011) and (Poulton and Canfield, 2011), suggesting a dominantly ferruginous deep ocean with euxinia limited to productive margins (see also (Reinhard et al., 2013) reviewed in (Lyons et al., 2014). Our data—specifically comparatively high Mo contents in the middle euxinic interval and suggestions from the Fe speciation data for at least intermittently oxic conditions above and below, perhaps at

some appreciable water depth given the fine-grained nature of the sediments—suggest an interval of relatively oxic marine conditions in the mid-Proterozoic. We freely admit that the depth, lateral extent, and concentrations of marine oxygenation are difficult to constrain and in no way imply a significant oxygenation event. These inferred conditions for the Velkerri Formation do, however, make it a particularly attractive target in our search for eukaryotic life—within a framework of both local and global redox and implied nutrient controls. Moreover, we should be able to infer qualitatively productively and organic matter preservation variations across local redox gradients, if those local controls dominated the eukaryotic signal strength. In other words, we looked for eukaryotic signals in facies expected to favor their production (oxic) and preservation (anoxic)—recognizing that anoxic bottom waters can record (with strong fidelity) eukaryotic production in shallow, overlying oxic waters. At the same time, proximal deeper anoxic waters can challenge shallow eukaryotic life through upward mixing of those waters.

Despite our careful, independent consideration of primary redox controls, biomarker data across the three intervals of the Velkerri Formation show no evidence for the presence of the sterane compounds that are diagnostic of eukaryotic life, even in areas with high TOC and suggestions of oxic deposition. In addition, there are no detectable levels of aryl isoprenoids, thus anoxygenic photosynthesis could not have been supported at least in this setting at this time (Johnston et al., 2009). The lack of aryl isoprenoids and C_{40} parent carotenoid markers in the Velkerri Formation contrasts biomarker evidence for green and purple sulfur bacteria found in the older Barney Creek Formation (Brocks et

al., 2005). We are left with the conclusion that euxinia was of relatively limited extent during deposition of the Velkerri Formation in the mid-Proterozoic but was still more widely present than in today's ocean, which is estimated to be euxinic over approximately 0.1% of the seafloor (Reinhard et al., 2013). While we recognize the need for more data, we might be able to surmise that euxinia was seldom shallow and abundant enough to support appreciable anoxygenic primary production via sulfide oxidation—particularly in open marine settings. The absence of eukaryotic signals in our samples—despite our careful search within an independent paleoenvironmental context—suggests that other controls such as long-term nutrient and oxygen deficiencies may have held complex life at bay pending the profound environmental changes that marked the later Proterozoic.

SUPPLEMENTARY

Degree of Pyritization

Degree of pyritization (DOP) provides an estimate to the extent of which Fe reacts with H_2S to form pyrite. We measure (DOP) as a complement to the Fe speciation data. DOP is defined as:

$$DOP = \frac{Fe_{Py}}{Fe_{Py} + Fe_{HCl}}, \quad (1)$$

where Fe_{HCl} is iron extracted through boiling approximately 100 mg of powdered sample for one minute in concentrated HCl before quenching with deionized water (Raiswell et al., 1988) and measuring using a spectrophotometer at 562 nm using ferrozine (Stookey, 1970). Fe_{Py} is determined by boiling approximately 100 mg of powdered sample in a solution of 40 mL of 1.0 M $CrCl_2$ and 20 mL of concentrated HCl for two hours under N_2

gas (Canfield et al., 1986). H_2S is evolved from the reaction and is carried by the N_2 to a trap solution comprised of 3 % Zinc Acetate and 10 % Ammonium Hydroxide. 10 mL of 6 M HCl is added to the trap solution to liberate the sulfur, and a 0.1 M KIO_3 solution is used to titrate. Fe_{Py} concentration is calculated stoichiometrically from measured sulfur values. It should be noted that concentrated HCl reacts with poorly reactive silicate Fe that is unreactive to H_2S even on long diagenetic time scales, making this an aggressive extraction technique (Raiswell et al., 1994). Consequently, DOP should provide conservative estimate of remaining reactive Fe, which has reacted (or can react) with H_2S to form pyrite.

Sulfur Isotopes

Sulfur isotopes measurements were performed on a ThermoScientific Delta V+ Isotope Ratio Mass Spectrometer coupled with a Costech 4010 Elemental Combustion System through a ThermoScientific ConFlow III interface. Three international reference materials: IAEA-S-1, IAEA-S-2, and IAEA-S-3 and were run with each sample set referenced to Vienna-Canyon Diablo Troilite (VCDT).

$\delta^{34}S$ values from pyrite show a total range of approx. 40‰. The lightest value, -12.9 ‰, occurs in the upper Velkerri. The associated large fractionation corresponds with Fe speciation data that reflect euxinic deposition. The heaviest value, +25.8 ‰, also occurs in the upper Velkerri and closely matches the isotopic composition inferred for Roper seawater sulfate (Muir et al., 1985).

For comparison, in modern sedimentary environments, the sulfur isotopic offset between pyrite and sulfate often ranges between 25-40 ‰ or more (Chambers and

Trudinger, 1979). As the majority of the samples in this study were heavy (enriched) and thus showed a small fractionation, it is likely that the water column had low sulfate concentrations (Lyons et al., 2000; Shen et al., 2002; Shen et al., 2003). Low sulfate levels and enriched pyrite $\delta^{34}S$ is consistent with previous hypotheses of a sulfate-minimum zone (Logan et al., 1995) and would only be intensified with high rates of primary production and rapid sedimentation.

Trace-metals: Vanadium

Vanadium (V) is another trace-metal that can act as an indicator for paleo-environments and is effectively captured in shales deposited in reducing basins. Under mildly reducing conditions, vanadium exists as V (IV) in the form of vanadyl (VO^{2-}) and hydroxyl ions ($VO(OH)_3^-$, $(VO(OH)_2)$. Strongly reducing conditions with dissolved H_2S will reduce V (IV) to V (III), making it insoluble as V_2O_3 or $V(OH)_3$, allowing it to be scavenged by organic matter and leading to V enrichment in sediments deposited under anoxic water column. However, unlike Mo, V uptake can initiate in the absence of sulfide in the water column. It should be noted that under oxic conditions, redox sensitive elements such as Mo, U, and V can be adsorbed in significant quantities onto with Mn and Fe oxyhydroxides, which are then exported to the sediment where the trace metals can be liberated and released from the sediments upon reductive dissolution of the Fe phases at or below the water-sediment interface (Emerson and Huested, 1991; Hastings et al., 1996; Tribovillard et al., 2006). This behavior is consistent with the crustal values observed for these trace-metals in the lower and upper Velkerri.

FIGURE CAPTION

Table 1. Data for total carbon (TC), total organic carbon (TOC), total inorganic carbon (TOC), and total sulfur (TS).

Table 2. Data for Fe proxies: Fe_{Py}, Fe_{NaAc}, Fe_{Dith}, Fe_{Ox}, Fe_{HR}, Fe_{HCl}, Fe_T, Fe_{HR}/Fe_T, Fe_{Py}/Fe_{HR}, and DOP. Fe_{Py}—pyrite iron; Fe_{NaAc}—sodium acetate, Fe_{Dith}—sodium dithionite, Fe_{Ox}—ammonium oxalate, Fe_{HR}—highly reactive iron; Fe_{HCl}—boiling HCl iron; Fe_T—total iron; DOP—degree of pyritization.

Table 3. Sulfur Isotopes $\delta^{34}S$, ND means non-detect.

Table 4. Data for trace-metal: Mn—manganese, Mo—molybdenum, U—uranium, V—Vanadium, Al—aluminum, TOC—total organic carbon.

Table 5. Weights of rock powder extracted and extract yields.

Table 1.

Depth (m)	TC (wt.%)	TIC (wt.%)	TOC (wt.%)	TS (wt.%)
441.62-.64	1.1	0.0	1.1	0.7
441.63-.71	1.4	0.2	1.2	1.1
443.17-.19	1.3	0.0	1.3	0.7
444.70-.72	0.9	0.0	0.9	1.9
445.12-.14	0.6	0.0	0.6	0.9
446.28-.30	0.7	0.0	0.7	1.2
447.10-.12	0.8	0.0	0.8	1.0
449.19-.21	1.4	0.5	0.9	0.8
450.77-.79	1.3	0.0	1.3	0.7
451.76-.78	0.8	0.0	0.8	0.9
452.14-.22	1.5	0.0	1.5	1.2
452.47-.49	2.6	1.2	1.4	0.3
453.42-.44	0.2	0.0	0.2	0.5
455.60-.62	0.5	0.0	0.5	0.6
457.42-.44	0.5	0.0	0.5	1.0
458.45-.47	0.8	0.0	0.8	0.8
461.30-.32	1.4	0.0	1.4	0.2
461.94-.96	0.7	0.0	0.6	0.4
462.11-.13	0.8	0.0	0.7	0.7
464.08-.10	1.0	0.0	1.0	0.4
465.66-.68	0.8	0.0	0.7	0.3
467.92-.94	0.8	0.0	0.8	0.9
469.00-.08	1.4	0.0	1.3	0.6
469.28-.30	0.8	0.0	0.8	0.6
472.39-.41	1.7	0.5	1.2	0.5
473.20-.22	1.7	0.0	1.7	0.9
474.10-.12	2.9	0.8	2.1	0.3
475.51-.53	2.3	0.7	1.5	0.7
477.34-.36	1.0	0.0	1.0	2.6
502.00-.02	0.6	0.0	0.6	1.2
508.32-.34	2.0	1.2	0.8	0.2
508.35-.44	1.4	0.0	1.4	0.2
509.28-.30	0.8	0.0	0.8	0.6
512.62-.64	1.0	0.0	1.0	0.4
514.01-.03	0.9	0.0	0.9	0.2

516.04-.06	1.2	0.1	1.1	0.2
516.08-.10	0.6	0.0	0.6	0.7
518.24-.26	0.6	0.0	0.6	0.7
558.92-.94	1.0	0.1	1.0	1.0
561.58-.64	1.2	0.0	1.2	0.3
562.75-.77	1.4	1.2	0.2	0.6
564.50-.52	1.5	0.0	1.4	1.1
570.32-.34	1.1	0.0	1.1	1.1
605.75-.77	1.8	0.9	1.0	1.6
607.91-.98	2.6	0.0	2.6	1.4
608.62-.64	1.0	0.0	1.0	3.1
662.62-.64	4.8	0.0	4.8	1.7
662.69-.71	4.2	0.4	3.7	1.4
663.72-.74	3.8	0.7	3.1	2.2
663.83-.91	5.0	0.0	5.0	2.3
664.44-.46	5.1	0.1	5.0	3.2
666.75-.77	6.2	0.0	6.2	1.7
705.65-.67	6.9	0.0	6.9	6.0
706.87-.96	7.8	0.0	7.8	5.1
707.00-.20	8.8	0.0	8.8	9.9
707.95-.97	6.8	0.0	6.7	3.5
709.13-.15	8.0	0.0	8.0	4.9
709.72-.74	7.9	0.0	7.9	5.4
724.58-.60	6.7	0.0	6.7	3.3
725.66-.68	7.7	0.0	7.6	5.2
725.76-.88	7.7	0.0	7.6	3.9
726.61-.63	8.1	0.0	8.1	5.8
727.74-.76	3.4	0.0	3.4	1.1
800.94-.96	7.3	0.0	7.3	2.0
801.76-.78	6.7	0.0	6.7	2.9
802.78-80	6.5	0.1	6.4	1.6
803.92-.94	6.0	0.0	6.0	2.0
804.71-.73	6.5	0.0	6.5	1.9
848.31-.33	4.0	0.0	4.0	1.5
849.04-.06	3.9	0.0	3.9	1.8
850.08-.10	4.6	0.0	4.6	1.4
851.34-.36	3.9	0.0	3.9	2.9
852.48-.50	2.5	0.0	2.5	1.3

852.68-.76	3.2	0.0	3.1	1.4
910.51-.53	2.7	0.1	2.6	1.6
911.53-.55	4.0	0.1	3.9	1.0
912.24-.26	2.7	0.0	2.6	2.7
913.56-.58	3.0	0.4	2.5	0.1
914.39-.41	3.0	0.0	2.9	0.7
929.80-.82	3.1	0.0	3.1	3.7
930.12-.14	3.7	0.0	3.6	2.9
931.24-.26	5.1	0.0	5.1	3.6
932.61-.63	5.0	0.0	4.9	2.3
932.88-.92	5.5	0.0	5.5	2.4
933.12-.14	5.3	0.2	5.0	1.7
1002.92-.94	0.2	0.0	0.2	0.0
1004.38-.40	0.1	0.0	0.1	0.0
1004.98-1005.13	3.6	3.4	0.2	0.0
1053.45-.47	0.1	0.0	0.1	0.3
1055.68-.72	0.1	0.0	0.1	0.0
1056.43-.45	0.2	0.0	0.2	0.0
1124.94-.98	3.8	0.0	3.8	0.7
1125.55-.57	3.4	0.0	3.4	0.5
1126.49-.51	3.2	0.0	3.2	0.5
1127.09-.11	4.1	0.0	4.1	0.9
1130.48-.50	0.2	0.0	0.2	0.0
1131.91-.98	0.1	0.0	0.1	0.0
1197.47-.49	0.3	0.0	0.3	0.1
1198.79-.81	0.4	0.0	0.4	0.1
1202.48-.50	0.3	0.0	0.3	0.1
1203.75-77	2.6	0.0	2.6	0.7
1204.36-.44	3.6	0.0	3.6	0.6
1205.18-.20	3.9	0.0	3.9	0.4
1217.67-.69	0.6	0.0	0.6	0.1
1219.78-.80	0.6	0.0	0.6	0.0
1222.53-.55	0.3	0.0	0.3	0.0
1225.72-.74	0.2	0.0	0.2	0.0
1242.14-.16	1.0	0.0	1.0	0.8

Table 2.

Depth (m)	Fe_{Py} (wt.%)	Fe_{NaAc} (wt.%)	Fe_{Dith} (wt.%)	Fe_{Ox} (wt.%)	Fe_{HR} (wt.%)
441.62-.64	1.0	0.05	0.00	0.72	1.8
441.63-.71	0.5	0.28	0.34	0.67	1.8
443.17-.19	1.3	0.03	0.49	0.92	2.7
444.70-.72	0.9	0.03	0.96	0.73	2.6
445.12-.14	0.7	0.02	0.06	0.94	1.8
446.28-.30	0.9	0.00	0.26	0.17	1.4
447.10-.12	1.4	0.01	0.62	0.33	2.4
449.19-.21	0.4	0.30	0.57	0.90	2.2
450.77-.79	0.3	0.31	0.00	1.40	2.0
451.76-.78	0.5	0.05	0.00	0.65	1.2
452.14-.22	2.5	0.06	0.37	0.36	3.3
452.47-.49	0.4	0.39	0.00	1.60	2.4
453.42-.44	0.5	0.02	0.98	0.26	1.8
455.60-.62	0.6	0.01	0.21	0.10	0.9
457.42-.44	0.3	0.01	0.62	0.33	1.2
458.45-.47	1.1	0.00	0.27	0.19	1.6
461.30-.32	0.3	0.22	0.09	0.00	0.6
461.94-.96	0.4	0.03	0.31	0.38	1.1
462.11-.13	0.3	0.05	0.00	0.55	0.9
464.08-.10	0.1	0.05	0.00	0.28	0.5
465.66-.68	0.1	0.04	0.03	0.33	0.6
467.92-.94	0.5	0.00	0.12	0.07	0.7
469.00-.08	0.4	0.12	0.20	0.23	0.9
469.28-.30	0.3	0.06	0.59	0.47	1.4
472.39-.41	0.3	0.07	0.01	0.01	0.4
473.20-.22	0.6	0.16	0.24	1.21	2.2
474.10-.12	0.2	0.42	0.12	1.81	2.5
475.51-.53	0.5	0.31	0.32	1.85	3.0
477.34-.36	1.6	0.02	0.57	0.38	2.5
502.00-.02	0.4	0.00	0.18	0.13	0.7
508.32-.34	0.3	0.33	0.39	1.44	2.5
508.35-.44	0.2	0.14	0.13	0.23	0.7
509.28-.30	0.4	0.02	0.13	0.09	0.6
512.62-.64	0.3	0.04	0.13	0.21	0.7
514.01-.03	1.6	0.01	0.00	0.57	2.1

516.04-.06	0.1	0.10	0.09	0.56	0.8
516.08-.10	0.1	0.02	0.15	0.14	0.4
518.24-.26	0.8	0.07	0.38	0.18	1.4
558.92-.94	0.7	0.30	0.52	0.61	2.1
561.58-.64	0.2	0.15	0.16	0.15	0.7
562.75-.77	0.7	0.15	0.37	2.12	3.4
564.50-.52	0.4	0.05	0.44	1.08	2.0
570.32-.34	0.4	0.37	0.34	0.71	1.9
605.75-.77	0.3	0.02	0.17	1.09	1.5
607.91-.98	1.2	0.33	0.25	0.70	2.5
608.62-.64	1.6	0.01	0.41	0.14	2.2
662.62-.64	0.7	0.22	0.24	0.05	1.3
662.69-.71	0.8	0.44	0.15	0.02	1.4
663.72-.74	1.2	0.07	0.00	0.08	1.3
663.83-.91	2.4	0.04	0.22	0.07	2.7
664.44-.46	2.2	0.00	0.00	0.05	2.2
666.75-.77	0.9	0.07	0.12	0.05	1.2
705.65-.67	2.7	0.13	0.00	0.13	2.9
706.87-.96	3.9	0.06	0.49	0.12	4.6
707.00-.20	5.1	0.07	0.56	0.02	5.8
707.95-.97	2.2	0.08	0.33	0.04	2.7
709.13-.15	2.1	0.05	0.50	0.06	2.7
709.72-.74	1.0	0.04	0.00	0.12	1.1
724.58-.60	2.8	0.02	0.71	0.17	3.7
725.66-.68	2.4	0.08	0.65	0.20	3.4
725.76-.88	1.6	0.03	0.00	0.00	1.7
726.61-.63	3.0	0.06	0.73	0.21	4.0
727.74-.76	0.8	0.00	0.16	0.05	1.0
800.94-.96	1.0	0.01	0.00	0.00	1.0
801.76-.78	1.3	0.03	0.54	0.04	1.9
802.78-80	1.1	0.06	0.03	0.03	1.2
803.92-.94	0.9	0.01	0.00	0.00	0.9
804.71-.73	1.3	0.05	0.00	0.02	1.4
848.31-.33	1.1	0.01	0.32	0.04	1.4
849.04-.06	1.0	0.01	0.30	0.04	1.4
850.08-.10	0.7	0.01	0.00	0.00	0.7
851.34-.36	2.5	0.20	0.54	0.11	3.4
852.48-.50	0.5	0.01	0.00	0.00	0.5

852.68-.76	0.6	0.02	0.00	0.00	0.6
910.51-.53	0.7	0.09	0.00	0.12	0.9
911.53-.55	0.4	0.09	0.00	0.10	0.6
912.24-.26	1.5	0.05	0.01	0.01	1.5
913.56-.58	0.3	0.32	0.00	0.12	0.8
914.39-.41	0.4	0.07	0.11	0.08	0.6
929.80-.82	1.4	0.25	1.52	0.10	3.3
930.12-.14	1.1	0.10	0.81	0.32	2.3
931.24-.26	1.1	0.36	1.49	0.10	3.1
932.61-.63	1.4	0.06	0.23	0.09	1.8
932.88-.92	0.7	0.01	0.00	0.00	0.7
933.12-.14	1.1	0.04	0.11	0.09	1.3
1002.92-.94	0.1	0.06	0.05	0.16	0.3
1004.38-.40	0.1	0.06	0.04	0.15	0.4
1004.98-1005.13	0.1	0.02	0.05	0.27	0.4
1053.45-.47	0.2	0.10	0.07	0.18	0.6
1055.68-.72	0.1	0.02	0.00	0.00	0.1
1056.43-.45	0.1	0.06	0.00	0.17	0.3
1124.94-.98	0.3	0.00	0.00	0.00	0.3
1125.55-.57	0.2	0.10	0.00	0.08	0.4
1126.49-.51	0.3	0.02	0.00	0.13	0.4
1127.09-.11	0.7	0.03	0.00	0.20	0.9
1130.48-.50	0.1	0.08	0.00	0.16	0.3
1131.91-.98	0.1	0.01	0.04	0.06	0.2
1197.47-.49	0.1	0.12	0.00	0.27	0.4
1198.79-.81	0.1	0.08	0.16	0.22	0.5
1202.48-.50	0.0	0.09	0.16	0.22	0.5
1203.75-77	0.4	0.04	0.13	0.14	0.7
1204.36-.44	0.3	0.01	0.00	0.00	0.3
1205.18-.20	0.2	0.02	0.08	0.11	0.4
1217.67-.69	0.1	0.04	0.03	0.12	0.2
1219.78-.80	0.1	0.04	0.04	0.16	0.3
1222.53-.55	0.2	0.00	0.01	0.07	0.3
1225.72-.74	0.2	0.04	0.01	0.12	0.4
1242.14-.16	1.0	0.01	0.80	0.70	2.5

Table 3.

Depth (m)	$\delta^{34}S$
441.62-.64	5.6
441.63-.71	19.8
443.17-.19	6.1
444.70-.72	3.8
445.12-.14	11.6
446.28-.30	0.3
447.10-.12	12.8
449.19-.21	ND
450.77-.79	5.5
451.76-.78	-1.5
452.14-.22	12.0
452.47-.49	ND
453.42-.44	13.3
455.60-.62	13.2
457.42-.44	15.6
458.45-.47	3.5
461.30-.32	18.0
461.94-.96	17.2
462.11-.13	14.4
464.08-.10	19.3
465.66-.68	23.0
467.92-.94	23.0
469.00-.08	16.5
469.28-.30	18.7
472.39-.41	11.1
473.20-.22	8.2
474.10-.12	18.6
475.51-.53	1.9
477.34-.36	1.1
502.00-.02	9.7
508.32-.34	20.8
508.35-.44	12.1
509.28-.30	23.2
512.62-.64	16.4
514.01-.03	10.8

516.04-.06	19.9
516.08-.10	3.5
518.24-.26	ND
558.92-.94	11.7
561.58-.64	17.4
562.75-.77	16.5
564.50-.52	13.1
570.32-.34	17.8
605.75-.77	20.8
607.91-.98	25.8
608.62-.64	14.2
662.62-.64	-7.9
662.69-.71	7.4
663.72-.74	-7.2
663.83-.91	12.9
664.44-.46	1.1
666.75-.77	-4.6
705.65-.67	6.5
706.87-.96	9.5
707.00-.20	-9.3
707.95-.97	7.5
709.13-.15	7.7
709.72-.74	9.3
724.58-.60	14.4
725.66-.68	17.3
725.76-.88	15.4
726.61-.63	11.6
727.74-.76	13.5
800.94-.96	ND
801.76-.78	24.0
802.78-80	24.3
803.92-.94	20.0
804.71-.73	17.0
848.31-.33	10.9
849.04-.06	10.0
850.08-.10	14.5
851.34-.36	12.5
852.48-.50	22.7

852.68-.76	16.3
910.51-.53	4.0
911.53-.55	8.2
912.24-.26	9.2
913.56-.58	7.6
914.39-.41	6.5
929.80-.82	18.3
930.12-.14	13.5
931.24-.26	14.4
932.61-.63	8.6
932.88-.92	11.3
933.12-.14	13.8
1002.92-.94	ND
1004.38-.40	ND
1004.98-1005.13	ND
1053.45-.47	9.5
1055.68-.72	ND
1056.43-.45	0.0
1124.94-.98	ND
1125.55-.57	5.6
1126.49-.51	ND
1127.09-.11	6.5
1130.48-.50	ND
1131.91-.98	ND
1197.47-.49	ND
1198.79-.81	ND
1202.48-.50	ND
1203.75-77	5.9
1204.36-.44	ND
1205.18-.20	6.9
1217.67-.69	ND
1219.78-.80	ND
1222.53-.55	ND
1225.72-.74	ND
1242.14-.16	12.0

Table 4.

Sample I.D.	Mn (ppm)	Mo (ppm)	Mo/TOC (ppm/wt.%)	U (ppm)	V (ppm)	Al wt.%
441.62-.64	278	3	2.3	2	78	9.7
441.63-.71	759	1	1.1	3	65	7.9
443.17-.19	318	1	0.9	2	70	8.3
444.70-.72	284	2	1.8	2	68	8.3
445.12-.14	177	1	1.8	2	63	8.3
446.28-.30	83	1	1.6	2	79	10.0
447.10-.12	158	1	1.6	2	77	9.7
449.19-.21	570	1	1.3	2	62	7.3
450.77-.79	467	1	0.8	2	61	7.5
451.76-.78	278	1	1.3	2	74	9.1
452.14-.22	512	2	1.5	3	130	12.6
452.47-.49	939	1	0.5	2	63	7.9
453.42-.44	259	1	4.6	2	68	9.0
455.60-.62	88	1	1.7	3	66	8.8
457.42-.44	149	1	1.4	2	62	8.3
458.45-.47	173	2	2.0	4	119	11.7
461.30-.32	305	1	0.6	2	66	7.9
461.94-.96	141	1	1.3	3	70	8.9
462.11-.13	214	1	1.2	2	69	9.1
464.08-.10	144	1	0.9	2	64	8.5
465.66-.68	137	1	1.2	3	85	10.8
467.92-.94	70	1	1.3	3	96	11.2
469.00-.08	288	2	1.6	3	77	9.5
469.28-.30	187	1	1.1	2	68	8.8
472.39-.41	501	1	0.8	2	82	9.2
473.20-.22	431	1	0.8	3	83	9.2
474.10-.12	703	1	0.6	2	68	7.2
475.51-.53	499	1	0.6	2	73	7.2
477.34-.36	108	3	3.0	3	97	9.0
502.00-.02	71	0	0.2	2	75	9.1
508.32-.34	322	1	1.0	2	70	8.5
508.35-.44	316	3	2.2	2	62	8.2
509.28-.30	79	1	1.5	3	89	10.8
512.62-.64	116	2	1.7	3	113	12.0
514.01-.03	127	1	1.1	2	86	8.1

516.04-.06	259	1	1.0	2	71	9.3
516.08-.10	74	1	1.9	3	79	9.4
518.24-.26	115	1	1.9	2	88	8.5
558.92-.94	235	1	1.3	3	70	7.8
561.58-.64	208	5	4.5	1	48	6.3
562.75-.77	532	1	3.6	2	65	7.7
564.50-.52	312	2	1.1	3	84	9.0
570.32-.34	240	1	1.0	3	68	6.4
605.75-.77	307	1	1.3	3	85	10.3
607.91-.98	672	1	0.3	3	34	4.0
608.62-.64	117	3	2.8	3	82	8.6
662.62-.64	74	11	2.3	4	397	5.7
662.69-.71	183	14	3.7	5	531	5.3
663.72-.74	270	6	2.0	4	239	5.0
663.83-.91	99	23	4.5	8	628	7.3
664.44-.46	98	8	1.5	4	311	5.0
666.75-.77	68	27	4.3	7	630	6.0
705.65-.67	92	47	6.9	16	393	5.0
706.87-.96	136	100	12.9	19	735	7.9
707.00-.20	109	71	8.1	20	402	4.5
707.95-.97	129	51	7.6	13	468	5.9
709.13-.15	61	33	4.2	11	383	4.9
709.72-.74	68	75	9.5	17	389	4.3
724.58-.60	97	30	4.5	8	397	5.9
725.66-.68	157	105	13.8	19	585	7.9
725.76-.88	98	73	9.5	17	408	5.6
726.61-.63	143	92	11.3	17	611	9.4
727.74-.76	111	17	5.2	6	363	7.5
800.94-.96	54	53	7.2	21	388	4.6
801.76-.78	52	44	6.6	16	365	7.2
802.78-80	125	43	6.8	17	293	4.6
803.92-.94	47	43	7.2	12	276	3.7
804.71-.73	90	35	5.4	14	280	4.4
848.31-.33	54	6	1.6	4	167	4.7
849.04-.06	73	4	0.9	4	198	5.0
850.08-.10	35	8	1.8	5	147	3.0
851.34-.36	140	18	4.5	7	367	7.0
852.48-.50	91	6	2.6	4	150	4.2

852.68-.76	109	1	0.4	6	141	3.3
910.51-.53	287	0	0.2	2	119	4.5
911.53-.55	326	1	0.2	5	183	5.4
912.24-.26	345	5	2.1	3	80	3.2
913.56-.58	947	0	0.2	1	65	3.5
914.39-.41	285	5	1.8	3	164	5.9
929.80-.82	153	10	3.3	7	141	4.2
930.12-.14	84	16	4.5	9	215	4.6
931.24-.26	84	10	2.0	10	267	4.4
932.61-.63	187	26	5.3	10	327	5.5
932.88-.92	84	34	6.1	13	234	4.1
933.12-.14	572	41	8.2	12	434	7.0
1002.92-.94	386	2	7.6	1	57	8.8
1004.38-.40	393	2	13.3	1	54	10.0
1004.98-1005.13	4875	3	11.0	3	17	1.6
1053.45-.47	316	2	11.3	1	40	7.1
1055.68-.72	231	1	11.9	2	43	6.6
1056.43-.45	310	1	8.2	1	44	8.1
1124.94-.98	86	2	0.6	4	39	5.5
1125.55-.57	86	1	0.4	2	45	7.2
1126.49-.51	107	2	0.6	2	41	7.3
1127.09-.11	124	3	0.8	3	58	7.5
1130.48-.50	180	1	6.2	2	52	7.5
1131.91-.98	270	7	67.3	4	67	6.6
1197.47-.49	198	1	2.9	2	64	7.1
1198.79-.81	203	1	2.0	2	74	8.5
1202.48-.50	233	2	5.1	2	89	9.5
1203.75-77	141	3	1.0	3	130	7.7
1204.36-.44	87	8	2.3	5	104	6.0
1205.18-.20	125	4	0.9	4	154	7.8
1217.67-.69	147	1	1.1	2	68	9.8
1219.78-.80	151	1	1.3	1	62	9.1
1222.53-.55	100	1	3.5	2	71	10.1
1225.72-.74	117	1	5.9	1	44	7.8
1242.14-.16	392	1	0.7	2	69	9.5

Table 5.

I.D.	452.14-.22	**TLE (mg)**	51.0	**Rock Powder (g)**	15.0951	gTOC
Age	1.45 Ga	**Sats (mg)**	8.5	**TC (wt.%)**	1.4925	0.22
Fm	Velkerri	**Aros (mg)**	6.4	**TIC (wt.%)**	0.0305	
	Roper	**Pols (mg)**	10.9	**TOC (wt.%)**	1.4620	
		Yield (mg extract/g rock)	3.4	**TS (wt.%)**	1.2290	

I.D.	508.35-.44	**TLE (mg)**	64.6	**Rock Powder (g)**	20.0246	gTOC
Age	1.45 Ga	**Sats (mg)**	13.5	**TC (wt.%)**	1.3992	0.28
Fm	Velkerri	**Aros (mg)**	3.9	**TIC (wt.%)**	0.0000	
	Roper	**Pols (mg)**	15.5	**TOC (wt.%)**	1.3992	
		Yield (mg extract/g rock)	3.2	**TS (wt.%)**	0.1925	

I.D.	561.58-.64	**TLE (mg)**	49.6	**Rock Powder (g)**	19.9847	gTOC
Age	1.45 Ga	**Sats (mg)**	22.4	**TC (wt.%)**	1.2137	0.24
Fm	Velkerri	**Aros (mg)**	7.7	**TIC (wt.%)**	0.0246	
	Roper	**Pols (mg)**	19.7	**TOC (wt.%)**	1.1891	
		Yield (mg extract/g rock)	2.5	**TS (wt.%)**	0.2918	

I.D.	607.91-.98	**TLE (mg)**	3.1	**Rock Powder (g)**	10.0180	gTOC
Age	1.45 Ga	**Sats (mg)**	1.0	**TC (wt.%)**	2.5864	0.26
Fm	Velkerri	**Aros (mg)**	1.4	**TIC (wt.%)**	0.0170	
	Roper	**Pols (mg)**	0.9	**TOC (wt.%)**	2.5694	
		Yield (mg extract/g rock)	0.3	**TS (wt.%)**	1.3598	

I.D.	663.83-.91	**TLE (mg)**	63.6	**Rock Powder (g)**	15.0340	gTOC
Age	1.45 Ga	**Sats (mg)**	10.9	**TC (wt.%)**	4.9845	0.75
Fm	Velkerri	**Aros (mg)**	9.4	**TIC (wt.%)**	0.0109	
	Roper	**Pols (mg)**	13.5	**TOC (wt.%)**	4.9736	
		Yield (mg extract/g rock)	4.2	**TS (wt.%)**	2.2619	

I.D.	706.87-.96	**TLE (mg)**	30.0	**Rock Powder (g)**	20.0740	gTOC
Age	1.45 Ga	**Sats (mg)**	11.3	**TC (wt.%)**	7.7920	1.56
Fm	Velkerri	**Aros (mg)**	8.0	**TIC (wt.%)**	0.0236	
	Roper	**Pols (mg)**	10.7	**TOC (wt.%)**	7.7684	
		Yield (mg extract/g rock)	1.5	**TS (wt.%)**	5.1013	

I.D.	725.76-.88	**TLE (mg)**	54.1	**Rock Powder (g)**	12.1587	gTOC
Age	1.45 Ga	**Sats (mg)**	2.1	**TC (wt.%)**	7.6681	0.93
Fm	Velkerri	**Aros (mg)**	3.2	**TIC (wt.%)**	0.0327	
	Roper	**Pols (mg)**	4.9	**TOC (wt.%)**	7.6354	
		Yield (mg extract/g rock)	4.4	**TS (wt.%)**	3.8549	

I.D.	852.68-.76	**TLE (mg)**	89.4	**Rock Powder (g)**	11.9698	gTOC
Age	1.45 Ga	**Sats (mg)**	2.3	**TC (wt.%)**	3.1500	0.37
Fm	Velkerri	**Aros (mg)**	9.2	**TIC (wt.%)**	0.0184	
	Roper	**Pols (mg)**	18.3	**TOC (wt.%)**	3.1316	
		Yield (mg extract/g rock)	7.5	**TS (wt.%)**	1.3662	

I.D.	932.88-.92	**TLE (mg)**	58.0	**Rock Powder (g)**	10.0066	gTOC
Age	1.45 Ga	**Sats (mg)**	36.1	**TC (wt.%)**	5.4929	0.55
Fm	Velkerri	**Aros (mg)**	12.1	**TIC (wt.%)**	0.0003	
	Roper	**Pols (mg)**	9.1	**TOC (wt.%)**	5.4926	
		Yield (mg extract/g rock)	5.8	**TS (wt.%)**	2.3869	

REFERENCES

Abbott, S. T., and Sweet, I. P., 2000, Tectonic control on third-order sequences in a siliciclastic ramp-style basin: an example from the Roper Superbasin (Mesoproterozoic), northern Australia: Australian Journal of Earth Sciences, v. 47, no. 3, p. 637-657.

Algeo, T. J., and Lyons, T. W., 2006, Mo–total organic carbon covariation in modern anoxic marine environments: Implications for analysis of paleoredox and paleohydrographic conditions: Paleoceanography, v. 21, no. 1.

Anbar, A. D., and Knoll, A., 2002, Proterozoic ocean chemistry and evolution: a bioinorganic bridge?: Science, v. 297, no. 5584, p. 1137-1142.

Bekker, A., Holland, H., Wang, P.-L., Rumble, D., Stein, H., Hannah, J., Coetzee, L., and Beukes, N., 2004, Dating the rise of atmospheric oxygen: Nature, v. 427, no. 6970, p. 117-120.

Brasier, M. D., and Lindsay, J. F., 1998, A billion years of environmental stability and the emergence of eukaryotes: New data from northern Australia: Geology, v. 26, no. 6, p. 555-558.

Brocks, J. J., Love, G. D., Summons, R. E., Knoll, A. H., Logan, G. A., and Bowden, S. A., 2005, Biomarker evidence for green and purple sulphur bacteria in a stratified Palaeoproterozoic sea: Nature, v. 437, no. 7060, p. 866-870.

Buick, R., Des Marais, D. J., and Knoll, A. H., 1995, Stable isotopic compositions of carbonates from the Mesoproterozoic Bangemall group, northwestern Australia: Chemical Geology, v. 123, no. 1–4, p. 153-171.

Calvert, S., and Pedersen, T., 1996, Sedimentary geochemistry of manganese; implications for the environment of formation of manganiferous black shales: Economic Geology, v. 91, no. 1, p. 36-47.

Calvert, S. E., and Pedersen, T. F., 1993, Geochemistry of Recent oxic and anoxic marine sediments: Implications for the geological record: Marine Geology, v. 113, no. 1–2, p. 67-88.

Canfield, D. E., Farquhar, J., and Zerkle, A. L., 2010, High isotope fractionations during sulfate reduction in a low-sulfate euxinic ocean analog: Geology, v. 38, no. 5, p. 415-418.

Canfield, D. E., Raiswell, R., and Bottrell, S. H., 1992, The reactivity of sedimentary iron minerals toward sulfide: American Journal of Science, v. 292, no. 9, p. 659-683.

Canfield, D. E., Raiswell, R., Westrich, J. T., Reaves, C. M., and Berner, R. A., 1986, The use of chromium reduction in the analysis of reduced inorganic sulfur in sediments and shales: Chemical Geology, v. 54, no. 1, p. 149-155.

Chambers, L., and Trudinger, P., 1979, Microbiological fractionation of stable sulfur isotopes: a review and critique: Geomicrobiology Journal, v. 1, no. 3, p. 249-293.

Emerson, S. R., and Huested, S. S., 1991, Ocean anoxia and the concentrations of molybdenum and vanadium in seawater: Marine Chemistry, v. 34, no. 3–4, p. 177-196.

Farrimond, P., Talbot, H. M., Watson, D. F., Schulz, L. K., and Wilhelms, A., 2004, Methylhopanoids: Molecular indicators of ancient bacteria and a petroleum correlation tool: Geochimica et Cosmochimica Acta, v. 68, no. 19, p. 3873-3882.

Froelich, P. N., Klinkhammer, G. P., Bender, M. L., Luedtke, N. A., Heath, G. R., Cullen, D., Dauphin, P., Hammond, D., Hartman, B., and Maynard, V., 1979, Early oxidation of organic matter in pelagic sediments of the eastern equatorial Atlantic: suboxic diagenesis: Geochimica et Cosmochimica Acta, v. 43, no. 7, p. 1075-1090.

Hastings, D. W., Emerson, S. R., and Mix, A. C., 1996, Vanadium in foraminiferal calcite as a tracer for changes in the areal extent of reducing sediments: Paleoceanography, v. 11, no. 6, p. 665-678.

Jackson, M., Sweet, I., Page, R., and Bradshaw, B., 1999, The South Nicholson and Roper Groups: evidence for the early Mesoproterozoic Roper Superbasin: Integrated Basin Analysis of the Isa Superbasin using seismic, well-log and geopotential data: an evaluation of the economic potential of the Northern Lawn Hill Platform, v. 1999.

Jackson, M., Sweet, I., and Powell, T., 1988, Petroleum geology and geochemistry of the Middle Proterozoic, McArthur Basin, Northern Australia. I: Petroleum potential: Aust. Petrol. Explor. Assoc. J., v. 28, no. 1988, p. 283.

Jackson, M. J., Powell, T. G., Summons, R. E., and Sweet, I. P., 1986, Hydrocarbon shows and petroleum source rocks in sediments as old as 1.7 [times] 109 years: Nature, v. 322, no. 6081, p. 727-729.

Jackson, M. J., and Raiswell, R., 1991, Sedimentology and carbon-sulphur geochemistry of the Velkerri Formation, a mid-Proterozoic potential oil source in northern Australia: Precambrian Research, v. 54, no. 1, p. 81-108.

Javaux, E. J., Knoll, A. H., and Walter, M. R., 2001, Morphological and ecological complexity in early eukaryotic ecosystems: Nature, v. 412, no. 6842, p. 66-69.

Johnston, D. T., Wolfe-Simon, F., Pearson, A., and Knoll, A. H., 2009, Anoxygenic photosynthesis modulated Proterozoic oxygen and sustained Earth's middle age: Proceedings of the National Academy of Sciences, v. 106, no. 40, p. 16925-16929.

Kah, L. C., Lyons, T. W., and Frank, T. D., 2004, Low marine sulphate and protracted oxygenation of the Proterozoic biosphere: Nature, v. 431, no. 7010, p. 834-838.

Kendall, B., Creaser, R. A., Gordon, G. W., and Anbar, A. D., 2009, Re–Os and Mo isotope systematics of black shales from the Middle Proterozoic Velkerri and Wollogorang formations, McArthur Basin, northern Australia: Geochimica et Cosmochimica Acta, v. 73, no. 9, p. 2534-2558.

Knoll, A. H., Javaux, E. J., Hewitt, D., and Cohen, P., 2006, Eukaryotic organisms in Proterozoic oceans: Philosophical Transactions of the Royal Society B: Biological Sciences, v. 361, no. 1470, p. 1023-1038.

Logan, G. A., Hayes, J., Hieshima, G. B., and Summons, R. E., 1995, Terminal Proterozoic reorganization of biogeochemical cycles: Nature, v. 376, no. 6535, p. 53-56.

Lyons, T. W., 1997, Sulfur isotopic trends and pathways of iron sulfide formation in upper Holocene sediments of the anoxic Black Sea: Geochimica et Cosmochimica Acta, v. 61, no. 16, p. 3367-3382.

Lyons, T. W., Luepke, J. J., Schreiber, M. E., and Zieg, G. A., 2000, Sulfur geochemical constraints on mesoproterozoic restricted marine deposition: lower Belt Supergroup, northwestern United States: Geochimica et Cosmochimica Acta, v. 64, no. 3, p. 427-437.

Lyons, T. W., and Reinhard, C. T., 2009, An early productive ocean unfit for aerobics: Proceedings of the National Academy of Sciences, v. 106, no. 43, p. 18045-18046.

Lyons, T. W., Reinhard, C. T., and Planavsky, N. J., 2014, The rise of oxygen in Earth/'s early ocean and atmosphere: Nature, v. 506, no. 7488, p. 307-315.

Lyons, T. W., Reinhard, C. T., and Scott, C., 2009, Redox Redux: Geobiology, v. 7, no. 5, p. 489-494.

Lyons, T. W., and Severmann, S., 2006, A critical look at iron paleoredox proxies: New insights from modern euxinic marine basins: Geochimica et Cosmochimica Acta, v. 70, no. 23, p. 5698-5722.

Muir, M., Donnelly, T., Wilkins, R., and Armstrong, K., 1985, Stable isotope, petrological, and fluid inclusion studies of minor mineral deposits from the McArthur Basin: Implications for the genesis of some sediment-hosted base metal mineralization from the Northern Territory: Australian Journal of Earth Sciences, v. 32, no. 3, p. 239-260.

Och, L. M., and Shields-Zhou, G. A., 2012, The Neoproterozoic oxygenation event: environmental perturbations and biogeochemical cycling: Earth-Science Reviews, v. 110, no. 1, p. 26-57.

Partin, C. A., Bekker, A., Planavsky, N. J., Scott, C. T., Gill, B. C., Li, C., Podkovyrov, V., Maslov, A., Konhauser, K. O., Lalonde, S. V., Love, G. D., Poulton, S. W., and Lyons, T. W., 2013, Large-scale fluctuations in Precambrian atmospheric and oceanic oxygen levels from the record of U in shales: Earth and Planetary Science Letters, v. 369–370, no. 0, p. 284-293.

Planavsky, N. J., McGoldrick, P., Scott, C. T., Li, C., Reinhard, C. T., Kelly, A. E., Chu, X., Bekker, A., Love, G. D., and Lyons, T. W., 2011, Widespread iron-rich conditions in the mid-Proterozoic ocean: Nature, v. 477, no. 7365, p. 448-451.

Poulton, S. W., and Canfield, D. E., 2005, Development of a sequential extraction procedure for iron: implications for iron partitioning in continentally derived particulates: Chemical Geology, v. 214, no. 3–4, p. 209-221.

-, 2011, Ferruginous Conditions: A Dominant Feature of the Ocean through Earth's History: Elements, v. 7, no. 2, p. 107-112.

Radke, M., and Welte, D., 1981, The methylphenanthrene index (MPI): a maturity parameter based on aromatic hydrocarbons: Advances in organic geochemistry, v. 1983, p. 504-512.

Raiswell, R., Buckley, F., Berner, R. A., and Anderson, T., 1988, Degree of pyritization of iron as a paleoenvironmental indicator of bottom-water oxygenation: Journal of Sedimentary Research, v. 58, no. 5.

Raiswell, R., Canfield, D., and Berner, R., 1994, A comparison of iron extraction methods for the determination of degree of pyritisation and the recognition of iron-limited pyrite formation: Chemical Geology, v. 111, no. 1, p. 101-110.

Raiswell, R., and Canfield, D. E., 1998, Sources of iron for pyrite formation in marine sediments: American Journal of Science, v. 298, no. 3, p. 219-245.

Rashby, S. E., Sessions, A. L., Summons, R. E., and Newman, D. K., 2007, Biosynthesis of 2-methylbacteriohopanepolyols by an anoxygenic phototroph: Proceedings of the National Academy of Sciences, v. 104, no. 38, p. 15099-15104.

Reinhard, C. T., Planavsky, N. J., Robbins, L. J., Partin, C. A., Gill, B. C., Lalonde, S. V., Bekker, A., Konhauser, K. O., and Lyons, T. W., 2013, Proterozoic ocean redox and biogeochemical stasis: Proceedings of the National Academy of Sciences, v. 110, no. 14, p. 5357-5362.

Sahoo, S. K., Planavsky, N. J., Kendall, B., Wang, X., Shi, X., Scott, C., Anbar, A. D., Lyons, T. W., and Jiang, G., 2012, Ocean oxygenation in the wake of the Marinoan glaciation: Nature, v. 489, no. 7417, p. 546-549.

Scott, C., and Lyons, T. W., 2012, Contrasting molybdenum cycling and isotopic properties in euxinic versus non-euxinic sediments and sedimentary rocks: refining the paleoproxies: Chemical Geology, v. 324, p. 19-27.

Scott, C., Lyons, T. W., Bekker, A., Shen, Y., Poulton, S. W., Chu, X., and Anbar, A. D., 2008, Tracing the stepwise oxygenation of the Proterozoic ocean: Nature, v. 452, no. 7186, p. 456-459.

Seifert, W. K., and Michael Moldowan, J., 1978, Applications of steranes, terpanes and monoaromatics to the maturation, migration and source of crude oils: Geochimica et Cosmochimica Acta, v. 42, no. 1, p. 77-95.

Shen, Y., Canfield, D. E., and Knoll, A. H., 2002, Middle Proterozoic ocean chemistry: evidence from the McArthur Basin, northern Australia: American Journal of Science, v. 302, no. 2, p. 81-109.

Shen, Y., Knoll, A. H., and Walter, M. R., 2003, Evidence for low sulphate and anoxia in a mid-Proterozoic marine basin: Nature, v. 423, no. 6940, p. 632-635.

Stookey, L. L., 1970, Ferrozine---a new spectrophotometric reagent for iron: Analytical chemistry, v. 42, no. 7, p. 779-781.

Summons, R., Taylor, D., and Boreham, C., 1994, Geochemical tools for evaluating petroleum generation in the Middle Proterozoic sediments of the McArthur Basin, Northern Territory, Australia: APEA JOURNAL, v. 34, p. 692-692.

Summons, R. E., Jahnke, L. L., Hope, J. M., and Logan, G. A., 1999, 2-Methylhopanoids as biomarkers for cyanobacterial oxygenic photosynthesis: Nature, v. 400, no. 6744, p. 554-557.

Taylor, S. R., and McLennan, S. M., 1985, The continental crust: its composition and evolution.

Tribovillard, N., Algeo, T. J., Lyons, T., and Riboulleau, A., 2006, Trace metals as paleoredox and paleoproductivity proxies: an update: Chemical Geology, v. 232, no. 1, p. 12-32.

Warren, J. K., George, S. C., Hamilton, P. J., and Tingate, P., 1998, Proterozoic source rocks: sedimentology and organic characteristics of the Velkerri Formation, Northern Territory, Australia: AAPG bulletin, v. 82, no. 3, p. 442-463.